Acta metall. Vol. 37, No. 3, pp. 909–916, 1989
Printed in Great Britain.

0001-6160/89 $3.00 + 0.00

EFFECTS OF NON-PLANARITY ON THE MIXED MODE FRACTURE RESISTANCE OF BIMATERIAL INTERFACES

A. G. EVANS[1] and J. W. HUTCHINSON[2]
[1]Materials Department, Univeristy of California, Santa Barbara, CA 93106 and [2]Division of Applied Sciences, Harvard University, Cambridge, MA 02138, U.S.A.

(*Received* 3 *June* 1988)

Abstract—The effects of non-planarity on the fracture resistance locus of interfaces has been investigated using a simple model of contacting facets along the crack surface. The contacts resist the motion of the crack surface by means of friction and locking and thereby modify the energy release rate G^1 at the crack front. The modified G^1 governs the effect of the contacting facets on the overall interface fracture resistance, G_i. The trends in G_i with phase angle of loading are found to be influenced largely by a non-dimensional parameter that determines the length of the contact zone. This parameter is, in turn, dependent on the amplitude of the undulations on the fracture interface as well as its intrinsic fracture resistance.

Résumé—Nous avons étudié les effets de la non-planéité sur les lieux de résistance à la rupture des interfaces en utilisant un modèle simple de facettes en contact le long de la surface de la fissure. Les contacts freinent le mouvement de la surface de la fissure par friction et blocage, et ils modifient donc la vitesse de perte d'énergie G^1 en tête de fissure. Cette vitesse G^1 modifiée régit l'effet des facettes en contact sur la résistance à la ruptue interfaciale totale, G_i. Les variations de G_i avec l'angle de phase de la mise en charge sont fortement influencées par un paramètre sans dimension qui détermine la longueur de la zone de contact. Ce paramètre, par contre, dépend de l'amplitude des ondulations sur l'interface de rupture comme de sa résistance intrinséque à la rupture.

Zusammenfassung—Der Einfluß der Unebenheit auf den Ort des Bruchwiderstandes von Grenzflächen wurde mit einem einfachen Modell kontaktierender Facetten entlang der Bruchfläche untersucht. Die Kontakte widerstehen der Bewegung der Rißoberfläche durch Reibung und Verankerung und verändern daher die Freisetzungsrate der Energie G^1 an der Rißfront. Die modifizierte Rate G^1 beherrscht den Einfluß der kontaktierenden Facetten auf den gesamten Bruchwiderstand der Grenzfläche G_i. Die Abhängigkeiten von G^1 von dem Phasenwinkel der Belastung werden größtenteils durch einen dimensionslosen Parameterbeeinflußt, der die Länge der Kontaktzone bestimmt. Dieser Parameter hängt wiederum von der Amplitude der Wellungen auf der Bruch-Grenzfläche und deren intrinsischem Bruchwiderstand ab.

1. INTRODUCTION

Many important interface fracture problems involve mixed mode (shear and opening) displacements along the crack surfaces, as exemplified by thin film decohesion [1–3] and fiber debonding in composites [4]. Subject to such displacements, interface fracture must be influenced by non-planarity of the interface and by the phase angle of loading, $\Psi = \tan^{-1}(K_{II}/K_I)$, where K_I and K_{II} are the Mode I and Mode II stress intensity factors. Typical interfaces are non-planar [5] (Fig. 1) and crack surface contact either at undulations or at facets along the interface crack can have an effect on the overall fracture resistance of the interface, G_i, especially at large phase angles. Such phase angle effects are illustrated in Fig. 2, which indicates the results of a fracture test on Al_2O_3 bonded with Ti. The upper, interface failure was caused by applied loading, with $\Psi \approx 0$. The lower crack in the Al_2O_3 parallel to the interface formed subsequently, caused by the residual stress in the Ti acting as a thin film. For this case, $\Psi \approx \pi/4$ [6] at the interface crack, whereupon the crack is diverted into the Al_2O_3 rather than propagating along the interface.

Trends in G_i with phase angle of loading are predicted in the present study for the case of a faceted interface. The simplest model of the process that provides insightful preliminary conclusions, illustrated in Fig. 3, consists of kinks along the crack surface. When the crack surfaces contact at the kinks, the stress intensities K^1 at the crack front differ from the applied values to an extent governed by the kink angle, the kink amplitude and the friction coefficient. The trends in K^1 with these variables provide one contribution to the increase in interface fracture resistance with phase angle of loading, as elaborated in the present article. Other possible influences on G_i, such as crack front deflections, plasticity etc. are not considered in this study.

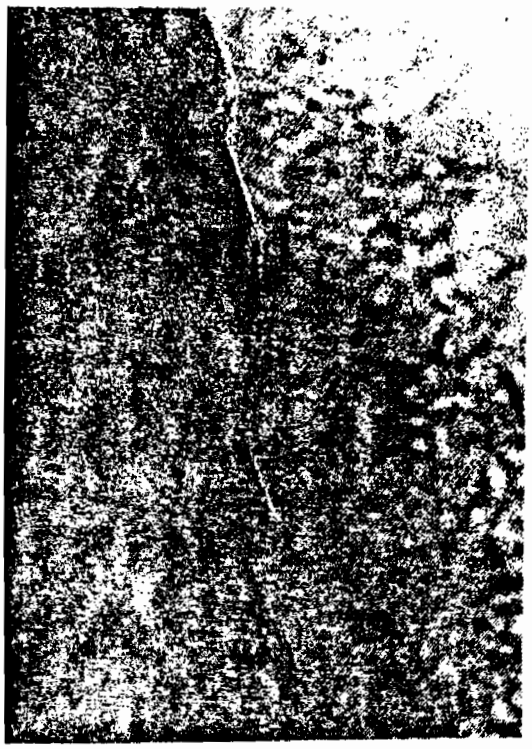

(a)

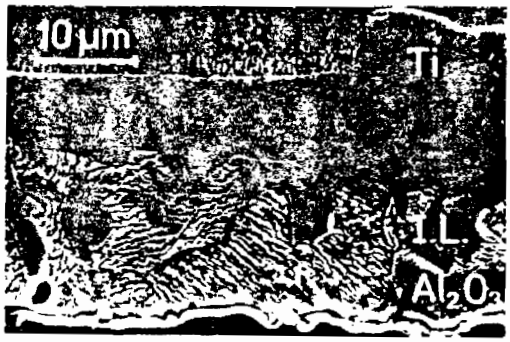

(b)

Fig. 1. Non-planar metal ceramic interfaces (courtesy M. Rühle). (a) Interface facets in the system Nb Al_2O_3. (b) Interface undulations in the system Ti Al_2O_3, with interphases of TiAl and Ti_3Al. Cracking occurs along the Al_2O_3 TiAl interface.

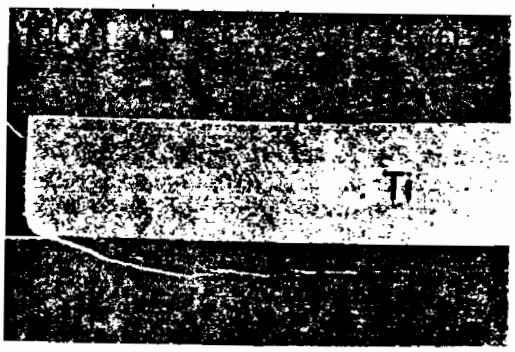

Fig. 2. The results of a fracture test on a Ti Al_2O_3 system. The upper, interface crack formed first upon loading. The lower crack in the Al_2O_3 formed subsequently, because of residual stress in the Ti (courtesy M. Rühle).

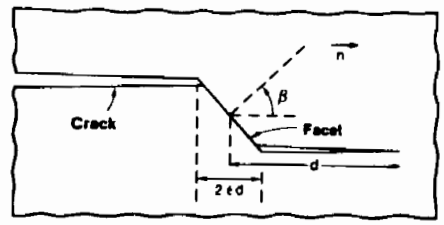

a) Basic Configuration

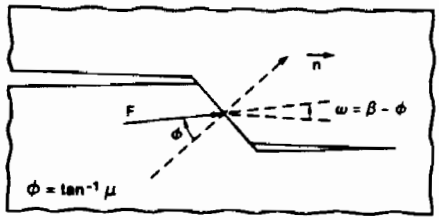

b) Frictional Force

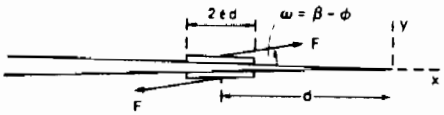

c) Elasticity Model

Fig. 3. The crack kink model used to analyze effects of crack surface contact. The loading in this case is $K_I > 0$ and $K_{II} < 0$.

2. THE BASIC MODEL

The model is developed for a thin interface between elastically homogeneous bodies with identical elastic properties. However, the general trends should be applicable to bimaterial interfaces, albeit that complex stress intensities should then be used [7]. The basic geometry involves a single kink [Fig. 3(a)] at angle β, along the crack surfaces at a distance, d, from the crack front. This geometric choice simulates each contact along a multiply facetted interface.

When the phase angle of loading allows contact at the kink, Coulomb friction is assumed to obtain with a friction angle

$$\phi = \arctan \mu \qquad (1)$$

where μ is the friction coefficient. Otherwise, elasticity exists throughout. An approximation for the effect of contact on the crack tip field invokes an inclined force, F, acting on the surfaces of a planar crack [Fig. 3(c)], with the inclination angle ω governed by ϕ and the kink angle β, (assuming that the faces of the facet are either sliding or on the verge of sliding) where

$$\omega = \beta - \phi. \qquad (2)$$

The derivation which follows assumes $0 < \beta < \pi/2$, as in Fig. 3. For kink angles in the range $\pi/2 < \beta < \pi$, all equations continue to be valid if ϕ is replaced by

$-\phi$ corresponding to the switch in direction of the friction force. The force is represented as a uniformly distributed traction acting over a characteristic microstructural length, $2\epsilon d$ [Fig. 3(c)]. This geometric choice allows the effect of contact to be expressed in terms of normal and shear forces, P and Q, respectively, acting over $2\epsilon d$

$$P = F\sin\omega, \quad Q = F\cos\omega \tag{3a}$$

or

$$Q + iP = Fe^{i\omega}. \tag{3b}$$

The uniformly distributed normal force causes a crack opening, u, at $x = -d$

$$u = [4(1-\nu)/\pi G]Pg(\epsilon) \tag{4a}$$

where [8]

$$g(\epsilon) = (2\epsilon)^{-1}\left\{\begin{array}{l}\sqrt{1+\epsilon} - \sqrt{1-\epsilon} + (1+\epsilon/2)\ln \\ \times [(\sqrt{1+\epsilon}+1)(\sqrt{1+\epsilon}-1)^{-1}] \\ -(1-\epsilon/2)\ln \\ \times [(1+\sqrt{1-\epsilon})(1-\sqrt{1-\epsilon})^{-1}]\end{array}\right\}$$

while the uniformly distributed shear force causes a relative shear displacement, v; at $x = -d$

$$v = \frac{4(1-\nu)}{\pi G}Qg(\epsilon) \tag{4b}$$

where G is the shear modulus and ν is Poisson's ratio. The crack surface displacements caused by contact are related to the forces by

$$u + iv = \frac{4(1-\nu)}{\pi G}g(\epsilon)Fe^{i\omega} \tag{5}$$

such that the *contact induced* contribution to the stress intensities at the crack *tip*, K^1, are

$$K_{II}^1 + iK_I^1 = \sqrt{2/\pi d}f(\epsilon)Fe^{i\omega} \tag{6}$$

where

$$f(\epsilon) = (\sqrt{1+\epsilon} - \sqrt{1-\epsilon})/\epsilon$$

and the subscripts I and II refer to the opening and shear modes, respectively.

The corresponding crack surface displacements at the contact site ($x = -d$) dictated by the *remote loads* are

$$v + iu = [4(1-\nu)/G]\sqrt{d/2\pi}(K_{II} + iK_I) \tag{7}$$

where K_I and K_{II} are the stress intensities associated with the applied loads.

3. CONTACT AND LOCKING CONDITIONS

The existence of crack surface contact and of frictional locking are influenced by the relative magnitudes of the phase angle of loading, Ψ, the friction angle, ϕ, and the kink angle, β. *Contact* along the *kink* only occurs when

$$u\cos\beta + v\sin\beta > 0. \tag{8}$$

Hence, by defining a characteristic stress intensity K^* as

$$K^* = -(K_{II}\cos\beta + K_I\sin\beta) \tag{9}$$

contact of the facet faces occurs when

$$K^* > 0 \tag{10a}$$

which, since $\tan\Psi = K_{II}/K_I$, is equivalent to

$$\pi - \beta < \Psi < 2\pi - \beta. \tag{10b}$$

Furthermore, *contact* along the *straight* crack surfaces occurs when

$$K_I < 0. \tag{11}$$

The basic contact conditions are mapped in Fig. 4. For present purposes, the condition, $K_I < 0$, is not meaningful. The analysis should only be used for positive K_I. A separate analysis would be needed for negative Mode I.

Frictional *locking* occurs when the tangential force along the kink, T, satisfies the inequality

$$T < \mu N \tag{12}$$

where N is the normal force. This condition can be expressed in terms of the forces P and Q using

$$N = Q\cos\beta + P\sin\beta \equiv \mathrm{Re}[(Q+iP)e^{-i\beta}] \tag{13a}$$

$$T = Q\sin\beta - P\cos\beta \equiv -\mathrm{Im}[(Q+iP)e^{-i\beta}]. \tag{13b}$$

Then, by noting that

$$N\sin\phi - T\cos\phi = \mathrm{Im}[(N - iT)e^{i\phi}] \equiv \mathrm{Im}[(Q+iP)e^{i(\phi-\beta)}] \tag{14}$$

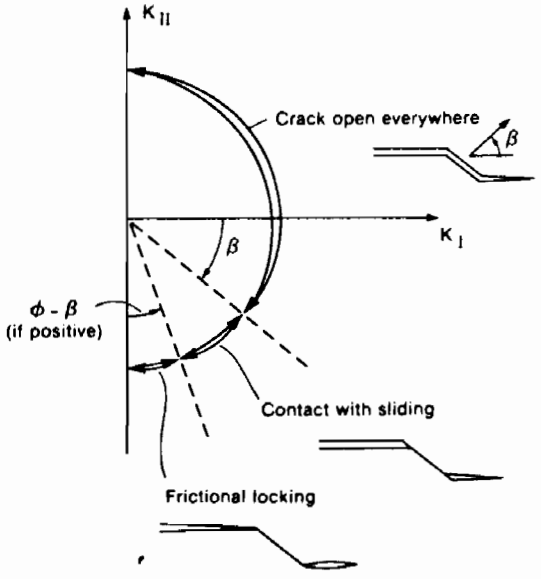

Fig. 4. A map of the sliding and locking conditions anticipated with the crack asperity. For present purposes, only $K_I > 0$ is relevant.

the locking condition becomes

$$\mathrm{Im}[(Q + iP)e^{i\phi - \beta)}] > 0 \tag{15a}$$

or, because locking requires that $u = v = 0$, (3b), (5) and (7) give

$$\mathrm{Im}[(K_{II} + iK_I)e^{i\phi - \beta)}] < 0. \tag{15b}$$

Consequently, since

$$K_{II} + iK_I = |K|e^{-i\psi - \pi/2)} \tag{16}$$

locking occurs when

$$\sin(\psi + \beta - \phi - \pi/2) > 0 \tag{17a}$$

or

$$\pi/2 - \beta + \phi < \psi < 3\pi/2 - \beta + \phi. \tag{17b}$$

Thus, if $\phi - \beta > 0$, a range of loading exists in which $K_I > 0$ and the facets are frictionally locked as mapped in Fig. 4.

4. INTERFACE FRACTURE RESISTANCE

The above conditions of contact and frictional locking provide insights concerning the analysis of the interface fracture resistance. For purposes of analysis, the spectrum of contacts must be simulated by means of a contact model. Two such models are presented, each providing a different perspective of the contact phenomenon. One model considers a single *row* of contacts with friction having a full spectrum of facet angles located at a *fixed* distance from the crack front. The fracture resistance can then be estimated, in principle, by summing over the number of rows within the contact zone. However, to accomplish this, an estimate of the zone size and of interaction between rows is needed. For this reason, a second *zone* model is developed that examines a simple contact condition at the facets, but more rigorously addresses the zone size and interactions that occur along the zone.

4.1. Single row model

Contact behavior at facets within a row is governed by the net displacements of the facet surfaces, derived from equations (5) and (7) as

$$(u + iv)e^{-i\beta} = 4\frac{1 - \upsilon}{G} \times \left[\sqrt{\frac{d}{2\pi}}(K_{II} + iK_I)e^{-i\beta} + \frac{g(\epsilon)}{\pi}Fe^{-i(\beta - \omega)}\right]. \tag{18}$$

When sliding contact occurs, $\beta - \omega = \phi$ and $\boldsymbol{u} \cdot \boldsymbol{n} = 0$ or, equivalently, $\mathrm{Re}\{u + iv)e^{-i\beta}\} = 0$. Thus, by (18), the resultant force across the facet faces is

$$F = \sqrt{\pi d/2}\, K^*/\cos\phi. \tag{19}$$

Inserting this expression for the force F into equation (6) and adding the stress intensities from the applied loads gives

$$K_{II}^1 + iK_I^1 = K_{II} + iK_I + h(\epsilon)e^{i\omega}K^*/\cos\phi \tag{20}$$

where $h(\epsilon) = f(\epsilon)/g(\epsilon)$ is the function plotted in Fig. 5. Consequently, the tip stress intensities are

$$K_I^1 = K_I + h(\epsilon)\sin(\beta - \phi)K^*/\cos\phi$$
$$K_{II}^1 = K_{II} + h(\epsilon)\cos(\beta - \phi)K^*/\cos\phi \tag{21}$$

and the strain energy release rate at the tip is

$$G^1 \equiv [(1 - \nu)/2G][(K_I^1)^2 + (K_{II}^1)^2]. \tag{22}$$

Noting that the effective energy release rate associated with the applied loads is

$$G = [(1 - \nu)/2G][K_I^2 + K_{II}^2] \tag{23}$$

the crack tip energy release rate becomes

$$G^1 = G + \frac{1 - \nu}{2G} \times \left\{\frac{2hK^*[K_I\sin(\beta - \phi) + K_{II}\cos(\beta - \phi)]}{\cos\phi} + \frac{h^2K^{*2}}{\cos^2\phi}\right\} \tag{24}$$

Thus, by (9)

$$\frac{\Delta G}{G} \equiv \Sigma(\phi, \beta, \psi, \epsilon) = +\,2h\frac{[(\sin\beta + \cos\beta\tan\psi)(\sin(\beta - \phi) + \cos(\beta - \phi)\tan\psi)]}{\cos\varphi(1 + \tan^2\psi)} - \frac{h^2(\sin\beta + \cos\beta\tan\psi)^2}{\cos^2\phi(1 + \tan^2\psi)} \tag{25}$$

where $\Delta G = G - G^1$ is the *reduction* in G, i.e. the shielding, caused by contact at the facet. (Recall that this equation, as well as all others above in-

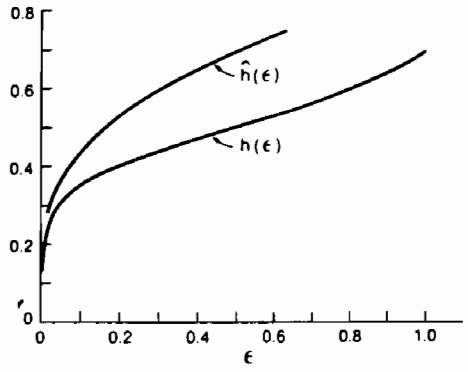

Fig. 5. Comparison of the functions $h(\epsilon)$ from the present approximate model and $\hat{h}(\epsilon)$ from the exact solution for a microcrack ahead of a macrocrack.

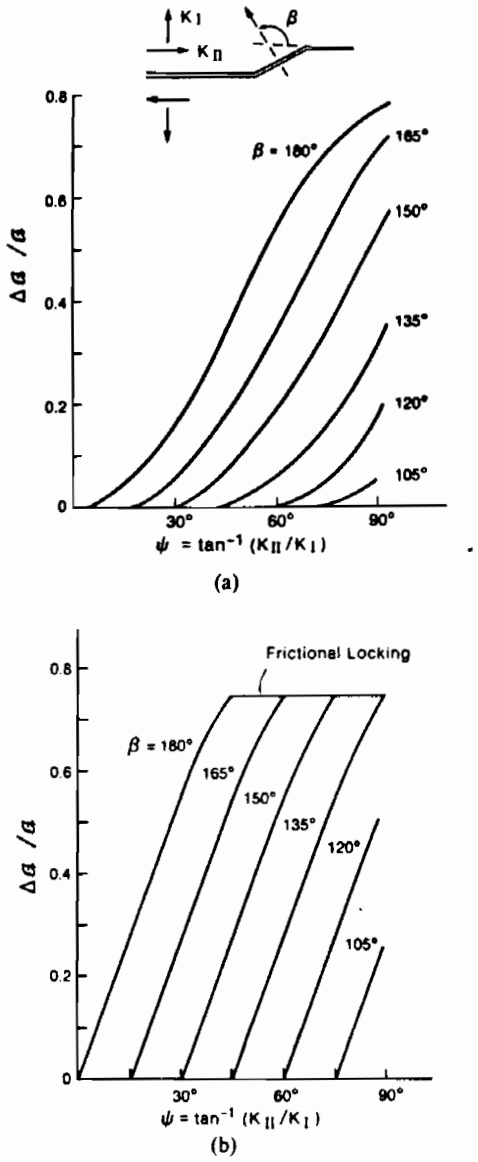

Fig. 6. (a) Reduction in crack tip release rate as a function of phase angle of loading for various kink orientations in the absence of friction ($h = 0.5$, $\phi = 0$). (b) Effect of friction ($\varphi = 45°$) on reduction in near tip energy release rate ($h = 0.5$).

volving ϕ, are limited to $0 < \beta < \pi/2$. For the range $\pi/2 < \beta < \pi$, ϕ must be replaced by $-\phi$.)

When *locking* occurs [equation (17), Fig. 4], the model gives

$$K_I^t/K_I = K_{II}^t/K_{II} = 1 - h(\epsilon) \tag{26}$$

and

$$G^t/G = [1 - h(\epsilon)]^2 \equiv \Omega(\epsilon) \tag{27}$$

which coincides with (21) and (24) when $\psi \to 3\pi/2 + \phi - \beta$. When locking occurs, the material along the kink behaves elastically and the tip stress intensities are equivalent to those for a microcrack of length $(1 - \epsilon)d$ at distance $2\epsilon d$ from the macrocrack tip [Fig. 3(c)]. The solution to this problem is known exactly and thus provides some calibration of the model. The solution is [9]

$$K_I^t/K_I = K_{II}^t/K_{II} = 1 - \hat{h}(\epsilon) \tag{28}$$

where $\hat{h}(\epsilon)$ is plotted in Fig. 5 along with $h(\epsilon)$. Noting the roles of h in (26) and $\hat{h}$ in (28), it is concluded that the present model underestimates somewhat the reduction in crack tip intensities due to contact at the facet. In the results calculated below, values of h are prescribed (rather than ϵ). To improve the accuracy of the model, these values may be identified with $\hat{h}$ for the purpose of evaluating the associated relative facet width ϵ.

Curves of $\Delta G/G$ vs ψ for various β as calculated from (25) are plotted in Fig. 6(a) with $\phi = 0$ and in Fig. 6(b) with $\phi = \pi/4$, in each case with $h = 0.5$. For loading combinations in the range shown ($0 < \psi < \pi/2$), contact does not occur for facet orientations with β less than $\pi/2$. The effect of friction is greatest when the facet angle is large, i.e. β greater than about $3\pi/4$. For the example in Fig. 6(b), frictional locking only occurs for $\beta > 3\pi/4$.

The interface fracture resistance is estimated based on consideration of a row of contacts with a uniform distribution of kink angles parallel to the front, ranging from 0 to π. (Kink angles with $\beta < 0$ or $\beta > \pi$ are unlikely because alternative, noninterfacial, fracture paths would normally obtain at facets having $\beta < 0$ or $\beta > \pi$.) For loading combinations with $0 \leqslant \psi \leqslant \pi/2$, the following conditions pertain. No contact occurs if

$$0 < \beta < \pi - \psi. \tag{29}$$

If $\phi + \psi < \pi/2$, no locking occurs at any β and the range of sliding contact is

$$\pi - \psi < \beta < \pi. \tag{30a}$$

If $\phi + \psi > \pi/2$, sliding contact occurs for

$$\pi - \psi < \beta < 3\pi/2 - \phi - \psi \tag{30b}$$

while locking occurs for

$$3\pi/2 - \phi - \psi < \beta < \pi. \tag{30c}$$

The *local* values of $\Delta G/G$ along the crack front are: zero for regions of no contact, Σ for contact without locking [equation (25)], and $1 - \Omega$ for locked kinks [equation (27)]. Interaction effects caused by neighboring kinks having different contact/locking conditions are thus neglected. With this simplification, an average value of ΔG along the crack front can be obtained by integration. For the case $\phi + \psi < \pi/2$, the fraction of noncontacting kinks is $1 - \psi/\pi$, while the fraction of contacting, non-locking kinks is ψ/π. Thus

$$\langle \Delta G \rangle / G = \frac{1}{\pi} \int_{\pi - \psi}^{\pi} \Sigma \, d\beta. \tag{31a}$$

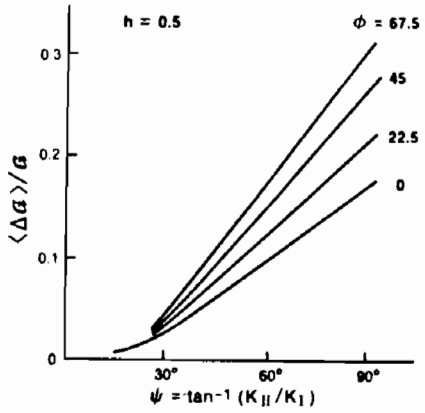

Fig. 7. Variation in crack shielding $\langle \Delta G \rangle$ with phase angle of loading caused by a row of contacts, for several friction angles ($h = 0.5$).

Similarly, for $\phi + \psi > \pi/2$

$$\langle \Delta G \rangle / G = \frac{1}{\pi} \int_{\pi - \psi}^{3\pi/2 - \phi - \psi} \Sigma \, d\beta + \left(\frac{\phi + \psi}{\pi} - \frac{1}{2} \right) (1 - \Omega). \quad (31b)$$

Curves of $\langle \Delta G \rangle / G$ as a function of ψ obtained from (31a, b) are plotted in Fig. 7 for several values of the friction angle ϕ. These curves were obtained using $h = 0.5$. The effect of different choices for h ranging over all realistic possibilities (cf. Fig. 5) is shown in Fig. 8. These results can be used to illustrate some of the issues involved in determining the extent of crack shielding.

It is firstly evident that there is only a moderate effect of the friction coefficient on crack shielding, within the usual range $0 < \phi < \pi/4$, because locking constitutes the greatest impediment to crack surface displacement. It is also noted from Fig. 5 that h remains quite large ($\gtrsim 0.2$) down to quite small values of ℓ (~ 0.05). Consequently, by simply summing $\langle \Delta G \rangle$ on parallel rows of nominally identical facets, all governed by equation (31), the net shielding must be sensitive to the number of rows and hence, the size of the contact zone. These insights suggest that a *zone* model which emphasizes the locking characteristics and explicitly incorporates the zone size should provide a more reasonable prediction of the effects of contact on the interface fracture resistance. Such a model is presented below.

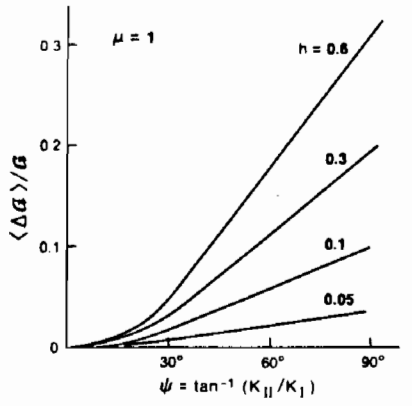

Fig. 8. The variation in crack shielding $\langle \Delta G \rangle$ with phase angle caused by a row of contacts, for a range of $h (\mu \equiv \tan \phi = 1)$.

4.2. Zone model

A zone model is developed for the simplified contact conditons depicted in Fig. 9 corresponding to $\beta = 0$ and $\phi = 0$ (no friction). Then, $K_I^t = K_I$ and the crack opening depends on K_I only, as given by

$$u(r) = 8(1 - \nu^2) K_I \sqrt{r} / \sqrt{2\pi} E \quad (32)$$

where r is the distance from the crack tip. Contacts exist over a zone length, L, that satisfies the condition

$$u(L) = H$$

where H is the height of the interface step (Fig. 9), such that

$$L = (\pi/32)[EH/(1 - \nu^2) K_I]^2. \quad (33)$$

Within the contact zone, the shear stresses and displacements are elastic and analogous to those associated with a linear array of microcracks (Fig. 9). Furthermore, in order to evalaute K_{II}^t, the microcracks can be simulated by a continuous linear spring model (Fig. 9) in which the stresses τ and

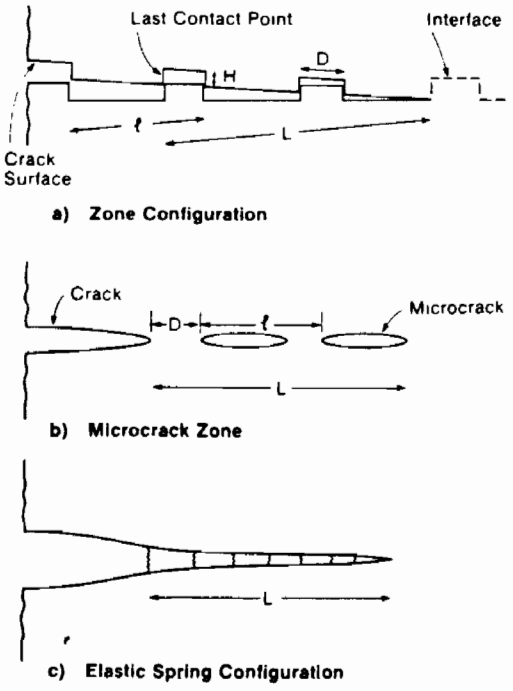

Fig. 9. A schematic illustrating the *zone* model used to determine trends in G_i with phase angle of loading.

Table 1. Interface properties for the glass polymer system

G_0	5 Jm^{-2}
E	70 GPa
H	10^{-6} m
$\chi \approx 0.1\, EH\, G_0$	$\approx 10^2$

displacements v are related by

$$v = \frac{8\tau l(1-\nu^2)\ln[1/\sin(\pi D/2l)]}{\pi E} \tag{34}$$

where l is the spacing between facet (microcrack) centers and D is the facet length (Fig. 9). This is the exact result for the additional shear displacement due to the presence of an infinite linear array of microcracks subject to remote shear stress τ parallel to the cracks [11, 12]. The linear spring model has been solved by Budiansky *et al.* [13]. For the present linear spring (34), the result of interest is

$$K_{II}^{t}/K_{II} = k(\alpha) \tag{35}$$

where

$$\alpha = \frac{(L-l)}{\ln[1/\sin(\pi D/2l)]} \tag{36}$$

and the function $k(\alpha)$ is given in Table 1 (as $1/\lambda$) in Ref. [13]. Plots of K_{II}^{t}/K_{II} vs D/l from (35) are shown in Fig. 10 for various numbers of microcracks $N(L = Nl)$. The result for one microcrack is the exact result from Ref. [9].

Using K_{II}^{t}/K_I and (35), the relation between the energy release rates is obtained as

$$G^{t}/G = \frac{1 + k^2(\alpha)\tan^2\psi}{1+\tan^2\psi}. \tag{37}$$

Further progress is achieved by combining equations (33) and (36) to give

$$\alpha = \frac{\pi EH^2(G^{t}/G)(1+\tan^2\psi)}{32(1-\nu^2)/G^{t}\ln[1/\sin(\pi D/2l)]}. \tag{38}$$

The basic trends in the fracture behavior of the interface with the phase angle of loading can be estimated by selecting the value of α at $\psi = 0$ as a reference value, α_0, and setting G^{t} equal to the fracture resistance of the interface G_0, such that

$$\alpha_0 = \frac{\pi(EH^2/G_0)}{32(1-\nu^2)\ln[1/\sin(\pi D/2l)]}. \tag{39}$$

The quantity α_0 contains the basic information concerning the interface and is thus a *material parameter*. The results contained in equations (35), (37), (38) and (39) can be combined to provide an expression for the crack shielding as

$$\Delta G/G = \frac{\tan^2\psi\{1 - k[\alpha_0(1+\tan^2\psi)(\Delta G/G+1)]\}}{1+\tan^2\psi}. \tag{40}$$

Specific trends in $\Delta G/G$ with ψ for various α_0 determined using equation (40) are plotted in Fig. 11.

It may be ascertained from Fig. 11 that two regimes exist: one at $\alpha_0 \gtrsim 1$, and the other when $\alpha_0 \lesssim 10^{-3}$. For the former, contact has the *maximum* effect on crack shielding, such that, $K_{II}^{t} \approx 0$ and

$$\Delta G/G = \frac{\tan^2\psi}{1+\tan^2\psi}. \tag{41}$$

For the latter, there is essentially no shielding when $\psi < \pi/2$. The significance of these two regimes may be appreciated by noting that undulating interfaces typically have geometry: $D/l \sim 1/2$, $H/l \sim 1/2$. Then α_0 becomes

$$\alpha_0 \approx 0.1/(EH/G_0)(1-\nu^2). \tag{42}$$

The governing material parameter is thus

$$\chi = EH/G_0.$$

This parameter, in essence, determines the contact zone dimensions, such that small values result in no contact and large values give full contact. Furthermore, the transition between these extremes occurs over a relatively small range of χ between ~ 10 and $\sim 10^{-3}$. Consequently, either a small value of the intrinsic interface toughness G_0 or a large amplitude

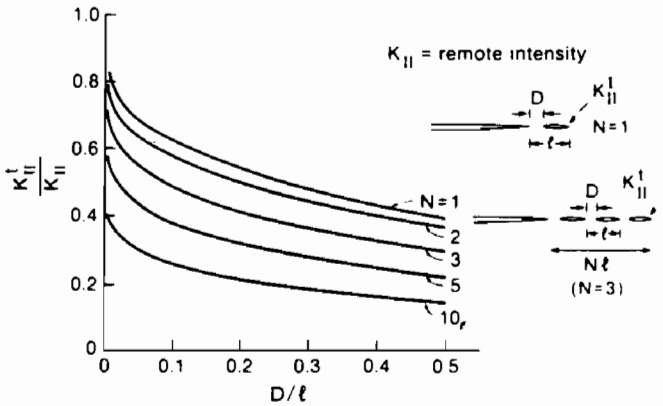

Fig. 10. Stess intensity at tip of lead microcrack in an array of equally spaced microcracks ahead of a macrocrack.

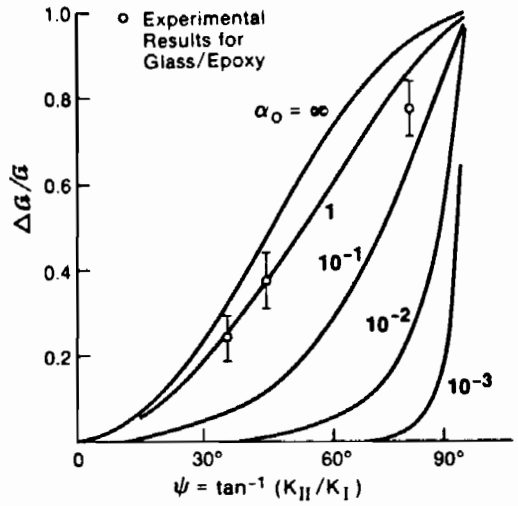

Fig. 11. Variation in crack shielding ΔG with phase angle of loading for various values of the contact zone parameter, α_0. Also shown are some experimental results obtained for a glass polymer interface [10].

undulation, H, may cause χ to become large, resulting in a mixed mode fracture resistance governed by equation (41), such that

$$G_i = G_0(1 + \tan^2 \psi). \tag{43}$$

Conversely, when H is small and/or G_0 is large, contact does not occur and $G_i \approx G_0$ for $\psi < \pi/2$.

5. COMPARISON WITH EXPERIMENT

Experimental results have been obtained in separate studies [10]. The results are in general accordance with the zone model predictions as depicted on Fig. 11 with $\alpha_0 \approx 1$ (or $\chi \approx 10$). Values of χ independently determined for the test interface are somewhat larger ($\chi \sim 10^2$, Table 1). This difference probably derives from the geometric simplicity of the zone model (Fig. 9). In particular, more realistic interface geometries would allow sliding of the edge of the contact zone and reduce the effective magnitude of the contact tractions, leading to improved correlations between theory and experiment. Some aspects of the discrepancy may also be associated with the modulus mismatch across the interface, which is not explicitly considered in the present analysis.

6. CONCLUDING REMARKS

The present analysis of contact effects on interface fracture resistance indicates that a simple zone model without friction predicts trends with the phase angle of loading qualitatively consistent with experimental results for a brittle interface that has no obvious plasticity associated with crack propagation. More complete experimental studies of contact zones would evidently allow further progress, and highlight deficiencies associated with the neglect of friction and with the present geometric simplification used to describe the interface. Studies of trends with the zone size parameter, EH/G_0, would be particularly insightful in this regard.

When the interface is subject to normal compression (negative K_I), a different analysis of fracture is needed. Nevertheless, it is already evident from the present analysis that sliding induces a positive K_i *at the tip* over a substantial range of compressions. Consequently, crack propagation will still be possible, as observed experimentally [10].

REFERENCES

1. A. G. Evans and J. W. Hutchinson, *Int. J. Solids Struct.* **20**, 455 (1984).
2. M. S. Hu, M. D. Thouless and A. G. Evans, *Acta metall.* **36**, 1301 (1988).
3. P. G. Charalambides, J. Lund, R. M. McMeeking and A. G. Evans, *J. appl. Mech.* In press.
4. P. G. Charalambides and A. G. Evans, *J. Am. Ceram. Soc.* To be published.
5. M. Rühle, unpublished research.
6. M. D. Drory, M. D. Thouless and A. G. Evans, *Acta metall.* **36**, 2019 (1988).
7. J. R. Rice, *J. appl. Mech.* **35**, 379 (1968).
8. H. Tada, P. Paris, G. Irwin, *The Stress Analysis of Cracks Handbook*. DEL Research Corp. (1973).
9. F. Rose, *Int. J. Fract.* **31**, 233 (1986).
10. H. C. Cao, Ph.D. thesis, Univ. of California, Berkeley (1988); H. C. Cao and A. G. Evans, *Mech. Mater.* In press.
11. W. T. Koiter, An infinite row of collinear cracks in an infinite elastic sheet, *Ingen. Arch.* **28**, 168 (1959).
12. M. Ortiz, *Int. J. Solids Struct.* **24**, 231 (1988).
13. B. Budiansky, J. C. Amazigo and A. G. Evans, *J. Mech. Phys. Solids.* **36**, 167 (1988).